Efficiency-Enhanced Reflective Nano-sieve-holograms

SAMIA OSMAN HAMID MOHAMMED [1], DONG ZHAO [1], SYED YASIR AZEEM [1], XIAO MING GOH[2], SHAWN J. TAN[2], JINGHUA TENG[2,3], KUN HUANG[1,*]

[1]*Department of Optics and Optical Engineering, University of Science and Technology of China, Hefei, Anhui 230026, China*
[2]*Institute of Materials Research and Engineering, Agency for Science, Technology and Research (A*STAR), 2 Fusionopolis Way, #08-03, Innovis, Singapore 138634*
[3] *Email address: jh-teng@imre.a-star.edu.sg*
** Corresponding author: huangk17@ustc.edu.cn*

Photon nanosieves, as amplitude-type metasurfaces, have been demonstrated usually in a transmission mode for optical super-focusing, display and holography, but the sieves with subwavelength size constrain optical transmission, thus leading to low efficiency. Here, we report reflective photon nanosieves that consist of metallic meta-mirrors sitting on a transparent quartz substrate. Upon illumination, these meta-mirrors offer the reflectance of ~50%, which is 2~45 times higher than the transmission of visible light through diameter-identical nanoholes. Benefiting from this configuration, a meta-mirror-based reflective hologram has been demonstrated with good consistence between theoretical and experimental results over the broadband spectrum from 500 nm to 650 nm, meanwhile exhibiting the total efficiency of ~7%. Additionally, if an additional high-reflectance layer is employed below these meta-mirrors, the efficiency can be enhanced further for optical anti-counterfeiting.

http://dx.doi.org/10.1364/OL.99.099999

Photon sieves composed of etched holes on an opaque film have been proposed firstly to reduce the focal spot size and alleviate high diffraction orders in soft X-ray and optical spectrum [1]. With the rapid development of nano-fabrication technology, the photon sieves have been demonstrated at nanoscale and worked as binary-amplitude metasurfaces for optical focusing [2, 3]. The photon-nano-sieves have the advantages of polarization independence and more degrees of freedom in design than the concentric rings in zone plates [4], which therefore enable more complex manipulation of light, such as hologram [2, 5], by arranging the locations of holes in a customized way. Due to the subwavelength feature of nanosieves, their related holograms usually support broadband operation [6]. In addition, the non-resonating mechanism of amplitude modulation allows the nanosieve hologram a wider spectrum than other metasurface devices with resonating nano-structures [7]. The nanosieve hologram also enables a large field of view for holographic display when combined with tunable phase realized by a spatial light modulator [8]. Beyond the circular shape, the rectangle nanosieves have also been proposed to control the geometric phase of a circularly polarized light by rotating the orientations of the rectangular nanosieves [9, 10], thus enabling full-color holography [11] and the generation of optical vortices [10, 12] in various electromagnetic spectrum such as X-ray and vacuum ultraviolet wavelengths [7, 13, 14].

All these reported nanosieves operate in a transmission mode, where optical transmission of light through the nanosieves is low because of the weak coupling between the propagating light and the waveguide modes supported within the nanoholes [2, 15]. Persistent efforts have been made to solve this efficiency issue. For example, a 15-layer MoS_2 film with a thickness of 10 nm can enhance the coupling for higher transmission meanwhile block the undesired background with strong exciton absorption [16]. The resulting hologram has a record-high efficiency of ~22%, where the contribution from the background light is also involved. Dielectric nanobricks located at only specially chosen positions, as an extension of classic photon nanosieves, are used to sieve the circularly polarized light with an additional geometric phase for realizing a wavelength- and polarization-sensitive hologram [17]. Although their demonstrated efficiency is only 2% at the wavelength of 670 nm due to small bandgap of the employed silicon, it indeed generalizes the concept of photon sieves, hereby suggesting new approaches for improving the efficiency of photon nanosieves.

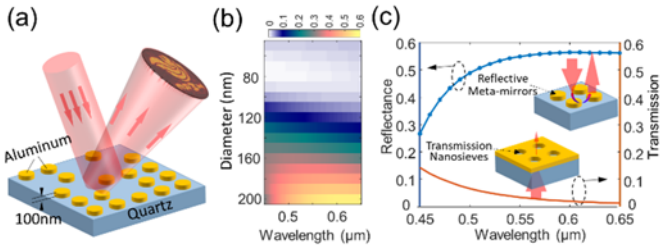

Fig. 1. (a) Sketch of reflective nanosieves composed of aluminum meta-mirrors that could sieve reflective photons for holography. (b) Reflectance of visible light from the 100 nm-height meta-mirrors with different diameters from 50 nm to 200 nm. (c) Comparison between the efficiency of the reflective nanosieves and the classic transmissive nanosieves. To make a fair comparison, the thicknesses of meta-mirrors and nanoholes are 100 nm and their periods are also kept with the same

value of 250 nm. Both diameters of the nano-mirrors and the nanoholes are 200 nm.

Here, we generalize the concept of photon nanosieve by proposing well-designed and location-optimized meta-mirrors that could sieve the reflected photons for holography. These aluminum meta-mirrors are located on a transparent quartz substrate, working as an analogue of transmissive photon nanosieves. The demonstrated meta-mirrors hologram has the experimental efficiency of ~7% over a broad visible spectrum, exhibiting an enhancement factor of ~3.5 compared with the previous transmissive nanosieves in similar dimensions.

The working principle of the proposed reflective nanosieves is sketched in Fig. 1(a), where the meta-mirrors with subwavelength diameters are used to reflect the incident light. By controlling the locations of these meta-mirrors, one customizes the expected optical field at the target plane. Under such a configuration, the efficiency of the meta-mirror is determined by its geometry, such as the diameter, the height and the period, as well as the material constructing the meta-mirror. Compared with other metals such as silver and gold, aluminum is employed here due to the lower cost and the less absorption of visible and ultraviolet light. For these aluminum meta-mirrors, their periods along *x* and *y* directions are chosen to be 250 nm, which is almost below a half of the entire visible wavelength. In addition, the heights of these aluminum meta-mirrors are optimized to be 100 nm, which is a good balance between optical efficiency and fabrication issues. For example, at the chosen height, the meta-mirrors with an optimized diameter of 200 nm could yield optical reflectance of ~50% at the interest wavelengths from 450 nm to 650 nm (Fig. 1(b)), which covers the preferred red, green and blue colors in optical display. If the thicker aluminum is used, its high-reflectance spectrum might shift out of this region due to the electromagnetic resonances. Similarly, the thinner aluminum cannot reflect light efficiently. Therefore, the reported meta-mirrors have a height of 100 nm and a diameter of 200 nm in a subwavelength period of 250 nm. Note that, the photons reflected by the meta-mirrors are sieved for manipulation of light, while the transmitted photons through the transparent substrate are not used in this work.

We compare the broadband reflectance for these meta-mirrors with the transmission for the classic photon nanosieves. For a fair comparison, the heights, diameters and periods are equal for both cases of meta-mirrors and nanosieves. The simulated results implemented by using the finite-difference time-domain (FDTD) method are presented in Fig. 1(c), which exhibits higher reflectance for the meta-mirrors than the transmission for the classic nanosieves. It reveals an enhancement factor of 2 at the 450-nm wavelength and ~45 at the 650-nm wavelength, hereby verifying the potential performance enhancement of the proposed meta-mirrors in theory.

Based on this meta-mirror platform, we design a hologram to verify the efficiency, as sketched in Fig. 2(a). In our simulation, the hologram has the pixel number of 800×800, where each pixel has a pitch of 250 nm×250 nm, thus leaving the total size of 200 μm×200 μm. The distance between the meta-mirror and the target plane is 1 mm, which is large enough for experimental recording of holographic image. To optimize such a hologram, we employ our previous modified genetic algorithm [2], where optical field diffracting from each meta-mirror can be approximated by using the field from a point source [6, 18]. During the optimization, the value of 1 for one pixel indicates that a meta-mirror exists at this pixel, while the value of 0 stands for the case of no meta-mirror. Thus, we can address every meta-mirror and superpose their electric fields coherently, hereby achieving the total field at the target plane. Considering that all these meta-mirrors have the same geometry, the total field depends on only the locations of meta-mirrors. Thus, the aim of this modified genetic algorithm is to optimize the positions of meta-mirrors so that the resulting field is convergent to the ideal pattern, *i.e.*, a lion with four letters "IMRE". Figures 2(b) and 2(c) show the designed meta-mirrors with nearly random distribution and the simulated intensity profile, respectively.

To verify it experimentally, we fabricate the designed meta-mirrors by using e-beam lithography (EBL) technique. A bare quartz substrate is coated with positive-tone resist polymethyl methacrylate (PMMA) at 3000 rpm to a thickness of 180 nm. The designed meta-mirrors patterns are created in PMMA by using EBL (Elionix ELS-7000) at an accelerating voltage of 100 kV and a beam current of 500 pA. Then, the pattern is developed with a 1:3 MIBK/IPA liquid, removing the exposed regions where the meta-mirrors should be located. After a dry blowing by N_2, the developed sample is deposited with a 100 nm-thick aluminum at a rate of 2 Å/s by using an electron-beam evaporator (Explorer Coating System, Denton Vacuum Inc). Finally, the expected meta-mirrors showed in Fig. 2(d) are formed by lift-off process. The achieved meta-mirrors have the diameters of 190 nm, which approaches tightly the designed value of 200 nm. The inhomogeneity at the surface of aluminum meta-mirrors is caused by the inevitable grain [19] during the deposition process.

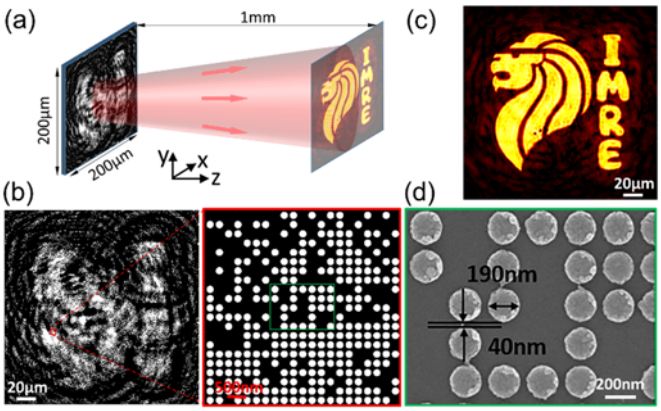

Fig. 2. (a) Sketch of meta-mirror-based hologram. The total size of the hologram is 200 μm×200 μm. (b) Designed meta-mirrors for hologram. The white region stands for the meta-mirrors. The right panel shows the zoomed-in pattern, which clearly give the details of meta-mirrors. (c) Simulated intensity profile at the target plane of z_0=1 mm at the wavelength of λ_0=532 nm. (d) Scanning-electron-microscopy (SEM) image of the fabricated meta-mirrors. It displays the region encircled within the green rectangle in (c).

The performance of the aluminum meta-mirror photon nanosieves is characterized by using the experimental set-up shown in Fig. 3(a). A supercontinuum laser (SuperK FIANIUM) is employed as the illuminating source with the tunable wavelength that is controlled by an acousto-optic modulator. A spherical lens and objective lens 1 (20X) is used to create a convergent wave that

works as a point source for illuminating the sample. Note that, the distance (labelled as d) between the point source and sample is slightly larger than z_0=1 mm, so that the holographic image is projected at the position $z_t=z_0 \cdot d/(d-z_0)$, which is called as the lensing effect of Fresnel hologram [6]. Meanwhile, the holographic image is magnified with a factor of $M=z_t/d$, facilitating its experimental capture. Considering the reflective operation mode, we put a 50:50 beam splitter between the sample and the objective 1 so that the reflected light can be collected by an objective lens 2 (10X) and then imaged onto a color camera (Thorlabs model).

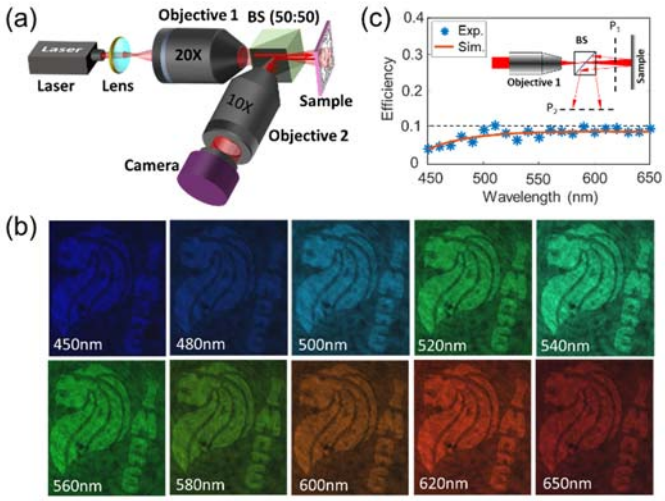

Fig. 3. (a) Experimental setup for the meta-mirror hologram characterization. BS: beam splitter. (b) Measured intensity profiles (raw data) at the exemplified wavelengths. (c). Simulated (curve) and experimental (asterisks) efficiency at the interested wavelengths.

Figure 3(b) shows the measured intensity profiles at the exemplified wavelengths from 450 nm to 650 nm. These holographic images cover blue, green, yellow and red colors, which makes this technique suitable for optical static display. It therefore confirms the validity of this hologram at a broadband spectrum of 200-nm width. Importantly, the imaging plane shifts at the different wavelength with a dispersion relationship of $z\lambda=z_0\lambda_0$, where z is the distance between the imaging plane at the wavelength λ and the meta-mirror hologram [6]. Due to the Fresnel imaging location of the demonstrated hologram [20], these reconstructed images have the same size, which is similar to the case of classic photon nanosieves. In addition, no aberration or distortion is observed at the recorded images, implying good quality of the holographic reconstruction.

To characterize the efficiency experimentally, we decrease the size of incident beam so that light is only shining within the area (*i.e.,* 200 μm ×200 μm) of the meta-mirror hologram, thus excluding optical reflectance of quartz outside the meta-mirror region. The incident power is recorded by a power meter (Thorlabs model) at the position P_1 (see the insert in Fig. 3(c)) and taken as I_{in}. Similarly, the power of the holographic image is measured by the same power meter at the position P_2 and labelled as I_{out}. Note that, the filling factor (defined by the ratio of the meta-mirror number in the hologram to the total number (i.e., 800×800) of all the pixels,) of our designed meta-mirror is only 20%. It means that 80% of the meta-mirror hologram is the quartz substrate, which leads to the undesired optical reflectance. Thus, the recorded power I_{out}=20%*I_{meta}+80%*I_{sub}, where I_{meta} and I_{sub} are assumed to be the reflected power from the meta-mirrors (100% filled in the region of 200 μm×200 μm) and the substrate (200 μm×200 μm), respectively. The signal light is extracted as $I_{signal}=I_{out}*\gamma$, where $\gamma=1/(1+4I_{sub}/I_{meta})$. The ratio I_{sub}/I_{meta} can be obtained by using the ratio of optical reflectance from the periodic meta-mirror and the bare substrate. Thus, the total efficiency of the meta-mirror hologram is $\eta=2*I_{signal}/I_{in}=2\gamma*\ I_{out}/I_{in}$, where the factor of 2 is multiplied because the 50:50 beam splitter only guides 50% of the signal light to the power meter. Figure 3(c) shows the experimental efficiency η, which agrees very well with the simulated efficiency that is evaluated by η=R*F*DE, where R is the reflectance of the meta-mirrors, the filling factor F=20% and the diffraction efficiency (defined by the ratio of the power of holographic image to the reflected energy purely from the meta-mirror) DE=75% over the entire spectrum of interest. As observed in Fig. 3(c), the efficiency of ~7% is obtained at the wavelengths from 500 nm to 650 nm. Compared with the efficiency of 2% for their counterpart classical photon nanosieves, the proposed reflective nanosieves have an enhanced efficiency with a factor of 3.5.

As a comparison among those efficiency-enhanced nanosieves, all of them are aimed at improving the transmission or reflectance of the sieved photons [16, 17]. But, as binary-amplitude devices, their theoretical limitation of optical efficiency is ~10% (note that, the MoS_2 nanosieves still have the efficiency of below 10% if the contribution from the background is removed). Therefore, the fundamental method to enhance the efficiency of nanosieves further is to introduce the phase modulation, which yields an efficiency limit of $\mathrm{sinc}^2(1/N)$ for a N-level phase [21]. If an additional metallic layer with high reflectance is employed below the meta-mirrors [22, 23], the current reflective nanosieves will introduce a binary-phase modulation of reflected light from the meta-mirror and the substrate, thus leading to an efficiency limitation of ~40%. Certainly, if the multi-level phase is employed, it will make the nanosieves behave like pure-phase metasurfaces [24].

In conclusion, we have proposed reflective photon nanosieves for holographic display. Much higher (by 3.5 times) efficiency than their counterpart transmission photon nanosieve is demonstrated experimentally. The hologram showed a broadband operation over 200 nm covering the visible range due to the subwavelength features of the meta-mirrors, with performance matching well with the simulation. The reflective photon nanosieve provides a potential technology for applications in optical display and anticounterfeiting [25].

Funding: K.H. thanks National Natural Science Foundation of China (Grant No. 12134013 and 61875181), USTC Research Funds of the Double First-Class Initiative (Grant No. YD2030002003), "the Fundamental Research Funds for the Central Universities" in China, the CAS Poineer Hundred Talents Program. J.T. thanks the A*STAR IRG grant A2083c0058 and CRF grant.

Acknowledgment: K. H. thanks the support from the University of Science and Technology of China's Centre for Micro and Nanoscale Research and Fabrication.

Disclosures: The authors declare no conflicts of interest.

References:

1. L. Kipp, M. Skibowski, R. L. Johnson, R. Berndt, R. Adelung, S. Harm, and R. Seemann, Nature **414**, 184-188 (2001).
2. K. Huang, H. Liu, F. J. Garcia-Vidal, M. Hong, B. Luk'yanchuk, J. Teng, and C.-W. Qiu, Nat. Commun. **6**, 7059 (2015).
3. Y. J. Liu, H. Liu, E. S. P. Leong, C. C. Chum, and J. H. Teng, Adv. Opt. Mater. **2**, 487-492 (2014).
4. S. Ishii, V. M. Shalaev, and A. V. Kildishev, Nano Lett. **13**, 159-163 (2013).
5. Z. Xu, L. Huang, X. Li, C. Tang, Q. Wei, and Y. Wang, Adv. Opt. Mater. **8**, 1901169 (2020).
6. K. Huang, H. Liu, G. Si, Q. Wang, J. Lin, and J. Teng, Laser Photonics Rev. **11**, 1700025 (2017).
7. J. Li, G. Si, H. Liu, J. Lin, J. Teng, and K. Huang, Opt. lett.**44**, 3418-3421 (2019).
8. J. Park, K. Lee, and Y. Park, Nat. Commun. **10**, 1304 (2019).
9. S. Mei, M. Q. Mehmood, S. Hussain, K. Huang, X. Ling, S. Y. Siew, H. Liu, J. Teng, A. Danner, and C.-W. Qiu, Adv. Fun. Mater. **26**, 5255-5262 (2016).
10. M. Mehmood, S. Mei, S. Hussain, K. Huang, S. Siew, L. Zhang, T. Zhang, X. Ling, H. Liu, and J. Teng, Adv. Mater. **28**, 2533-2539 (2016).
11. M. Pu, X. Li, X. Ma, Y. Wang, Z. Zhao, C. Wang, C. Hu, P. Gao, C. Huang, H. Ren, X. Li, F. Qin, J. Yang, M. Gu, M. Hong, and X. Luo, Sci. Adv. **1**, e1500396 (2015).
12. X. Ma, M. Pu, X. Li, C. Huang, Y. Wang, W. Pan, B. Zhao, J. Cui, C. Wang, and Z. Zhao, Sci. Rep. **5**, 10365 (2015).
13. L. Zhang, S. Mei, K. Huang, and C.-W. Qiu, Adv. Opt. Mater. **4**, 818-833 (2016).
14. D. Zhao, Z. Lin, W. Zhu, H. J. Lezec, T. Xu, A. Agrawal, C. Zhang, and K. Huang, Nanophotonics (2021).
15. A. Roberts, J. Opt. Soc. Am. A **4**, 1970-1983 (1987).
16. Z. Wang, G. Yuan, M. Yang, J. Chai, Q. Y. Steve Wu, T. Wang, M. Sebek, D. Wang, L. Wang, S. Wang, D. Chi, G. Adamo, C. Soci, H. Sun, K. Huang, and J. Teng, Nano Lett. **20**, 7964-7972 (2020).
17. D. Frese, B. Sain, H. Zhou, Y. Wang, L. Huang, and T. Zentgraf, Nanophotonics (2021).
18. K. Huang, F. Qin, Hong Liu, H. Ye, C. W. Qiu, M. Hong, B. Luk'yanchuk, and J. Teng, Adv. Mater. **30**, 1704556 (2018).
19. A. Taguchi, N. Hayazawa, K. Furusawa, H. Ishitobi, and S. Kawata, J. Raman Spectrosc. **40**, 1324-1330 (2009).
20. K. Huang, in *Chirality, Magnetism and Magnetoelectricity*, edited by E. Kamenetskii (Springer Nature Switzerland AG, 2021).
21. D. A. Buralli, G. M. Morris, and J. R. Rogers, Appl. Opt. **28**, 976-983 (1989).
22. S. Sun, K.-Y. Yang, C.-M. Wang, T.-K. Juan, W. T. Chen, C. Y. Liao, Q. He, S. Xiao, W.-T. Kung, and G.-Y. Guo, Nano Lett.**12**, 6223-6229 (2012).
23. G. Zheng, H. Mühlenbernd, M. Kenney, G. Li, T. Zentgraf, and S. Zhang, Nat. Nanotechnol. **10**, 308-312 (2015).
24. K. Huang, Z. Dong, S. Mei, L. Zhang, Y. Liu, H. Liu, H. Zhu, J. Teng, B. Luk'yanchuk, J. K. Yang, and C. Qiu, Laser Photonics Rev. **10**, 500-509 (2016).
25. K. Huang, J. Deng, H. S. Leong, S. L. K. Yap, R. B. Yang, J. Teng, and H. Liu, Laser Photonics Rev. **13**, 1800289 (2019).

Full references:

1. L. Kipp, M. Skibowski, R. L. Johnson, R. Berndt, R. Adelung, S. Harm, and R. Seemann, "Sharper images by focusing soft X-rays with photon sieves," Nature **414**, 184-188 (2001).
2. K. Huang, H. Liu, F. J. Garcia-Vidal, M. Hong, B. Luk'yanchuk, J. Teng, and C.-W. Qiu, "Ultrahigh-capacity non-periodic photon sieves operating in visible light," Nat. Commun. **6**, 7059 (2015).
3. Y. J. Liu, H. Liu, E. S. P. Leong, C. C. Chum, and J. H. Teng, "Fractal Holey Metal Microlenses with Significantly Suppressed Side Lobes and High-Order Diffractions in Focusing," Adv. Opt. Mater. **2**, 487-492 (2014).
4. S. Ishii, V. M. Shalaev, and A. V. Kildishev, "Holey-Metal Lenses: Sieving Single Modes with Proper Phases," Nano Lett. **13**, 159-163 (2013).
5. Z. Xu, L. Huang, X. Li, C. Tang, Q. Wei, and Y. Wang, "Quantitatively Correlated Amplitude Holography Based on Photon Sieves," Advanced Optical Materials **8**, 1901169 (2020).
6. K. Huang, H. Liu, G. Si, Q. Wang, J. Lin, and J. Teng, "Photon-nanosieve for ultrabroadband and large-angle-of-view holograms," Laser Photonics Rev. **11**, 1700025 (2017).
7. J. Li, G. Si, H. Liu, J. Lin, J. Teng, and K. Huang, "Resonance-free ultraviolet metaoptics via photon nanosieves," Optics letters **44**, 3418-3421 (2019).
8. J. Park, K. Lee, and Y. Park, "Ultrathin wide-angle large-area digital 3D holographic display using a non-periodic photon sieve," Nat. Commun. **10**, 1304 (2019).
9. S. Mei, M. Q. Mehmood, S. Hussain, K. Huang, X. Ling, S. Y. Siew, H. Liu, J. Teng, A. Danner, and C.-W. Qiu, "Flat Helical Nanosieves," Adv. Fun. Mater. **26**, 5255-5262 (2016).
10. M. Mehmood, S. Mei, S. Hussain, K. Huang, S. Siew, L. Zhang, T. Zhang, X. Ling, H. Liu, and J. Teng, "Visible-Frequency Metasurface for Structuring and Spatially Multiplexing Optical Vortices," Adv. Mater. **28**, 2533-2539 (2016).
11. M. Pu, X. Li, X. Ma, Y. Wang, Z. Zhao, C. Wang, C. Hu, P. Gao, C. Huang, H. Ren, X. Li, F. Qin, J. Yang, M. Gu, M. Hong, and X. Luo, "Catenary optics for achromatic generation of perfect optical angular momentum," Sci. Adv. **1**, e1500396 (2015).
12. X. Ma, M. Pu, X. Li, C. Huang, Y. Wang, W. Pan, B. Zhao, J. Cui, C. Wang, and Z. Zhao, "A planar chiral meta-surface for optical vortex generation and focusing," Scientific Reports **5**, 10365 (2015).
13. L. Zhang, S. Mei, K. Huang, and C.-W. Qiu, "Advances in Full Control of Electromagnetic Waves with Metasurfaces," Adv. Opt. Mater. **4**, 818-833 (2016).
14. D. Zhao, Z. Lin, W. Zhu, H. J. Lezec, T. Xu, A. Agrawal, C. Zhang, and K. Huang, "Recent advances in ultraviolet nanophotonics: from plasmonics and metamaterials to metasurfaces," Nanophotonics (2021).
15. A. Roberts, "Electromagnetic Theory of Diffraction by a Circular Aperture in a Thick, Perfectly Conducting Screen," J. Opt. Soc. Am. A **4**, 1970-1983 (1987).
16. Z. Wang, G. Yuan, M. Yang, J. Chai, Q. Y. Steve Wu, T. Wang, M. Sebek, D. Wang, L. Wang, S. Wang, D. Chi, G. Adamo, C. Soci, H. Sun, K. Huang, and J. Teng, "Exciton-Enabled Meta-Optics in Two-Dimensional Transition Metal Dichalcogenides," Nano Letters **20**, 7964-7972 (2020).
17. D. Frese, B. Sain, H. Zhou, Y. Wang, L. Huang, and T. Zentgraf, "A wavelength and polarization selective photon sieve for holographic applications," Nanophotonics (2021).
18. K. Huang, F. Qin, Hong Liu, H. Ye, C. W. Qiu, M. Hong, B. Luk'yanchuk, and J. Teng, "Planar Diffractive Lenses: Fundamentals, Functionalities, and Applications," Adv. Mater. **30**, 1704556 (2018).
19. A. Taguchi, N. Hayazawa, K. Furusawa, H. Ishitobi, and S. Kawata, "Deep-UV tip-enhanced Raman scattering," J. Raman Spectrosc. **40**, 1324-1330 (2009).
20. K. Huang, "Chirality and Antiferromagnetism in Optical Metasurfaces," in *Chirality, Magnetism and Magnetoelectricity*, E. Kamenetskii, ed. (Springer Nature Switzerland AG, 2021).
21. D. A. Buralli, G. M. Morris, and J. R. Rogers, "Optical performance of holographic kinoforms," Applied Optics **28**, 976-983 (1989).
22. S. Sun, K.-Y. Yang, C.-M. Wang, T.-K. Juan, W. T. Chen, C. Y. Liao, Q. He, S. Xiao, W.-T. Kung, and G.-Y. Guo, "High-efficiency broadband anomalous reflection by gradient meta-surfaces," nano Letters **12**, 6223-6229 (2012).
23. G. Zheng, H. Mühlenbernd, M. Kenney, G. Li, T. Zentgraf, and S. Zhang, "Metasurface holograms reaching 80% efficiency," Nat. Nanotechnol. **10**, 308-312 (2015).
24. K. Huang, Z. Dong, S. Mei, L. Zhang, Y. Liu, H. Liu, H. Zhu, J. Teng, B. Luk'yanchuk, J. K. Yang, and C. Qiu, "Silicon multi-meta-holograms for the broadband visible light," Laser Photonics Rev. **10**, 500-509 (2016).
25. K. Huang, J. Deng, H. S. Leong, S. L. K. Yap, R. B. Yang, J. Teng, and H. Liu, "Ultraviolet Metasurfaces of ≈80% Efficiency with Antiferromagnetic Resonances for Optical Vectorial Anti-Counterfeiting," Laser & Photonics Rev. **13**, 1800289 (2019).